Energy-Aware Ergodic Search: Continuous Long-Term Exploration for Multi-agent Systems

Adam Seewald[1], Marvin Chancán[1], Cameron J. Lerch[1], Hector Castillo[1], Aaron M. Dollar[1], and Ian Abraham[1]

***Abstract*——**

***Index Terms*—Motion and Path Planning; Energy and Environment-Aware Autonomation.**

I. INTRODUCTION

Robotic exploration is a recurring problem in different scenarios. It typically involves coverage path planning (CPP), which deals with deriving robots' trajectories that traverse every point in a given space [1–3]. Within CPP, ergodic search is a recent and promising direction [4–17], as it enhances the efficiency of traditional CPP by optimizing the time a robot spends in a given region w.r.t. an information measure. As a consequence, ergodic search derives trajectories so that the robots spend more time in areas with high information density while quickly passing areas with low information density [13, 18]. The user can specify areas of interest, e.g., where the robots should spend more time exploring in a search and rescue scenario [14], where the robots should collect more data in a precision agriculture scenario [16], etc.

Past literature has been studying ergodic search in manipulation [8], tactile sensing [15], stochastic dynamics [7, 17], distributed information [5], time optimality [14], and active learning [4]. Ergodic search for multi-agent systems [9, 10] has been applied in conjunction with low-information sensors [10–12], swarms control [9], obstacles [11], and decentralized systems [12]. Ergodic search has been proven successful in use cases involving urban environments [13] and information gathering [6]. While past literature includes ergodic search in a variety of settings, energy constraints have not been studied yet. Partly due to these constraints, the prospect of achieving long-term exploration that is continuous and considers a spatial distribution is currently hampered.

Canonical ergodic search indeed derives continuous exploration [5, 15, 19], but it is physically not possible to continue exploring on a single battery charge. Scenarios involving CPP, however, often require that the space is covered continuously. This work enhances the current ergodic search literature by incorporating more traditional energy-aware CPP approaches [20–25], battery- and energy-aware planning [26–29], and planning of energy tradeoffs [30, 31]. It answers the question: "*Is it possible to tradeoff battery and coverage quality so that there is at least one agent exploring the space at all times*"?

[1]A. S., M. C., C. J. L., H. C., A. M. D., and I. A. are with the Department of Mechanical Engineering and Materials Science, Yale University, CT, USA. Email: adam.seewald@yale.edu;

To answer the question, our approach derives an abstract battery model [32] for battery state of charge (SoC) estimation at future time instances. We first adapt canonical ergodic search to multi-agent ergodic search. We utilize the formulation in the following to propose energy-aware ergodic search or ergodic search under battery constraints. The exploration is continuous and runs long-term, employing a finite horizon framework reminiscent of a model predictive controller formulation with an empirically determined horizon [29]. Data from both simulations and real-world experiments show the impact of our newly proposed energy-aware ergodic search. We show that we can effectively explore a space guaranteeing that there is always one agent exploring, that the spatial distribution is satisfied, and that the exploration is continuous and long-term (see Section IV).

The remainder of the paper is then structured as follows. Sec. II formulates the problem of multi-agent continuous ergodic search. Sec. III discusses the methods for both the canonical ergodic search and a battery model enhanced ergodic search. Sec. V concludes and proposes future directions.

II. PROBLEM FORMULATION

This work addresses the problem of exploring a bounded space with multiple agents, continuously, and proportionally to a spatial distribution. In the remainder of the text, we will use the term "continuously" to indicate that there is at least one agent that is exploring the space at all times.

Canonical ergodic search [4–8, 18, 19] does not deal with continuous exploration. It derives an agent's control – or analogously multiple agents control [9–13] – so that its trajectory maximizes an ergodic metric defined in the spectral domain [33].

Problem II.1 (Ergodic search)**.** Consider a bounded space $\mathcal{Q} \subset \mathbb{R}^D$ of dimension D with $D \in \mathbb{N}_{>0}$ and a spatial distribution ϕ. *Ergodic search problem* is the problem of deriving a control action $\mathbf{u}(t) \in \mathcal{U} \subset \mathbb{R}^V$ with $V \in \mathbb{N}_{>0}$ so that the trajectory $\mathbf{q}(t) \in \mathcal{Q}$ is proportional to the spatial distribution ϕ.

Here the notation $\mathbb{R}$ and $\mathbb{N}$ indicates reals and naturals, $\mathbb{N}_{>0}$ strictly naturals. Bold notation is used for vectors.

We extend the canonical ergodic search problem to multi-agent continuous ergodic search, i.e., exploration with multiple agents under spatial distribution and battery constraints.

Problem II.2 (Multi-agent continuous ergodic search)**.** Consider a set of n agents $\boldsymbol{\alpha} := \{\alpha_1, \alpha_2, \dots, \alpha_n\}$, a bounded

space $\mathcal{Q}$, and a spatial distribution ϕ similar to Problem II.1. *Multi-agent continuous ergodic search problem* is the problem of deriving each agent ${}^{j}\alpha$ control action ${}^{j}\mathbf{u}(t)$ so that its trajectory ${}^{j}\mathbf{q}(t)$ is proportional to the spatial distribution ϕ on a continuous time horizon.

We will provide a solution to Problem II.2 (see Sec. III), assuming that there are one or more areas in $\mathcal{Q}$ – namely, charging stations – where the agents $\boldsymbol{\alpha}$ can land and recharge the battery, e.g., using wireless charging (see Sec. IV).

III. METHODS

In this section, we discuss the methods utilized in this work for continuous exploration with multiple agents and proportionally to a spatial distribution

We discuss how to achieve the latter in Sec. III-A and the former in Sec. III-B.

A. Ergodic search

To derive an agent's trajectory proportionally to a spatial distribution, canonical ergodic search first requires defining the distribution ϕ.

For the purposes of this, in both Problem II.1 and II.2, let us consider a Gaussian mixture model (GMM)

$$\phi(\boldsymbol{\delta}, \mathbf{q}) := \sum_{k=1}^{m} \delta_k \, \mathcal{N}(\mathbf{q} \,|\, \mu_k, \Sigma_k), \tag{1}$$

composed of m Gaussians. Each has a covariance matrix $\Sigma_k \in \mathbb{R}^{D \times D}$, a center $\mu_k \in \mathcal{Q}$, and a positive mixing coefficient $\delta_k \in \boldsymbol{\delta}$ such that the sum of the δs is less or equal to one. They indicate how well is each Gaussian in the GMM considered.

The goal of the ergodic search is to minimize an ergodic metric [18]

$$\mathcal{E}(\boldsymbol{\delta}, \mathbf{q}(t)) := \frac{1}{2} \sum_{k \in \mathcal{K}} \Lambda_k \big(c_k(\mathbf{q}(t)) - \phi_k(\boldsymbol{\delta})\big)^2, \tag{2}$$

where ϕ_k are coefficients derived utilizing the Fourier series on the spatial distribution ϕ and c_k on the trajectory $\mathbf{q}(t)$. They are detailed in Equation (6) and (4) respectively. Λ_k is a weight factor. That is, if

$$\Lambda_k = (1 + \|k\|^2)^{(-D-1)/2}, \tag{3}$$

lower frequencies have more weight [5]. $\mathcal{K} \in \mathbb{N}^D$ is a set of index vectors that covers $[K] \times \cdots \times [K] \in \mathbb{N}^{K^D}$ where K is a given number of frequencies including the fundamental frequency [33]. The notation $[K]$ indicates positive naturals up to K.

The coefficients c_k are derived using the Fourier series basis function. If we consider the trigonometric form, they can be expressed

$$c_k(\mathbf{q}(t)) := \int_{\mathcal{T}} \frac{1}{L^D} \prod_{d \in [D]_{>0}} \big(\cos(k_d \, \mathbf{q}_d(\tau) \, \psi) \\ - i \sin(k_d \, \mathbf{q}_d(\tau) \, \psi) \big) \, d\tau/t, \tag{4}$$

where ψ is $2\pi/L$ for a given period $L \in \mathbb{R}_{>0}$, i is the imaginary unit, k_d is the dth item of k, and $\mathbf{q}_d$ the dth item of $\mathbf{q}$.

$\mathcal{T}$ is built so that the integration is between $\tau = t_0$ and t, and the notation $[D]_{>0}$ indicates strictly positive naturals up to D.

c_k is evaluated per each k in $\mathcal{K}$ in Eq. (2).

To derive the coefficients ϕ_k, let us consider the GMM model in Eq. (1) on a search space $\mathcal{Q}$. The space is further bounded to a symmetric set $[-L/2, L/2]^D$ since the Gaussians are symmetric about the zero axes. The resulting new model is then

$$\Phi(\boldsymbol{\delta}, \mathbf{q}) := \sum_{d \in [2^D]_{>0}} \sum_{k=1}^{m} \delta_k \, \mathcal{N}(\mathbf{q} \,|\, A_d \mu_k, A_d \Sigma_k A_d^T)/2^D, \tag{5}$$

where $A_d \in \mathbb{R}^{D \times D}$ are linear transformation matrices [33]. Let us call the integrand in Eq. (4) $c : \mathcal{Q} \longrightarrow \mathbb{R}^K$. It maps the space to the spectral domain. The equivalent of Eq. (4) for the spatial distribution can be then expressed

$$\phi_k(\boldsymbol{\delta}) := \int_{\mathcal{Q}} \Phi(\boldsymbol{\delta}, \mathbf{q}) \, c(\mathbf{q}) \, d\mathbf{q}. \tag{6}$$

$\mathcal{Q}$ is built so that the integration is within the points of the bounded symmetric set $\mathbf{q} \in [-L/2, L/2]^D$.

ϕ_k is evaluated per each k in $\mathcal{K}$ in Eq. (2).

Let us first formulate the solution for Problem II.1, borrowed by canonical ergodic search. If the agent's dynamics is described by a generic differential equation $\dot{\mathbf{q}}(t) = f\big(\mathbf{q}(t), \mathbf{u}(t)\big)$, an optimal control problem (OCP) that selects an ergodic control action can be formulated as [17]

$$\min_{\mathbf{q}(t), \mathbf{u}(t)} \int_{\mathcal{T}} \mathbf{u}(\tau)^T R \mathbf{u}(\tau) \, d\tau + \mathcal{E}(\boldsymbol{\delta}, \mathbf{q}(t)), \tag{7a}$$

$$\text{s.t. } \dot{\mathbf{q}} = f(\mathbf{q}(t), \mathbf{u}(t)), \tag{7b}$$

$$\mathbf{q}(t) \in \mathcal{Q}, \, \mathbf{u}(t) \in \mathcal{U}, \tag{7c}$$

$$\mathbf{q}(t_0), \mathbf{q}(t_f) \text{ are given}, \tag{7d}$$

where the ergodic metric is derived in Eq. (2), $R \in \mathbb{R}^{V \times V}$ is a control penalizing diagonal positive-definite matrix, and t_0, t_f are respectively the first and last time instants. $\mathcal{T}$ is $[t_0, t_f)$.

To formulate the solution to Problem II.2, let us first extend the OCP in Eq. (7) to multi-agent systems [10]. Eq. (7a) becomes

$$\min_{\square} \frac{1}{n} \sum_{k=1}^{n} \left(\int_{\mathcal{T}_k} {}^{k}\mathbf{u}(\tau)^T R_k \, {}^{k}\mathbf{u}(\tau) \, d\tau + \mathcal{E}(\boldsymbol{\delta}, {}^{k}\mathbf{q}(t)) \right), \tag{8}$$

where the ergodic metric and the control penalizing term R_k are now agent-specific. The term $\square$ is ${}^{1}\mathbf{q}(t), {}^{2}\mathbf{q}(t), \ldots,$ ${}^{n}\mathbf{q}(t), {}^{1}\mathbf{u}(t), {}^{2}\mathbf{u}(t), \ldots {}^{n}\mathbf{u}(t)$. $\mathcal{T}_k$ is $[{}^{k}t_0, {}^{k}t_f)$, i.e., different agents might have different duration.

Let us consider a vector $\mathbf{b} \in \mathbb{R}^3$ – which is detailed later in Sec. III-B – whose trajectory $\mathbf{b}(t)$ describes the battery metrics' evolution in time. If $\mathbf{b}_{\text{SoC}}$ is the value of the vector that expresses the battery SoC, the expression in Eq. (8) might select ergodic metrics corresponding to trajectories that are impossible to traverse in the $\mathbf{b}_{\text{SoC}} \in (0, 1]$ domain, i.e., one or more agents' state at $\mathbf{q}(t_f)$ will not satisfy Eq. (7d).

In order to satisfy the battery SoC domain and always keep at least one agent exploring, an OCP must satisfy an additional constrain

$$\exists k \in [n] \text{ s.t. } {}^{k}\mathbf{b}_{\text{SoC}}(t_f) \in (0, b_f], \tag{9}$$

Fig. 1: . . . .
. . . .
. . . .
. . . .
. . . .
. . . .
. . . .
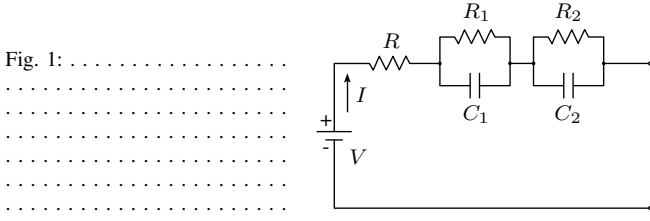
where $b_f \in (0,1) \subset \mathbb{R}_{>0}$ is a given desired battery SoC at the final time instant.

Finally, let us consider the realistic assumption that the optimization horizon $N \in \mathbb{R}_{>0}$ is known and is, e.g., an empirically collected value that corresponds to one of the agents' discharge times (see Sec. IV).

The OCP that provides a solution to Problem II.2 can be formulated as

$$\min_{\square} \frac{1}{n} \sum_{k=1}^{n} \int_{\mathcal{T}_k} {}^{k}\mathbf{u}(\tau)^T R_k \, {}^{k}\mathbf{u}(\tau) \, d\tau, \tag{10a}$$

$$\text{s.t. } {}^{1}\dot{\mathbf{q}}(t) = f_1({}^{1}\mathbf{q}(t), {}^{1}\mathbf{u}(t)), \ldots, {}^{n}\dot{\mathbf{q}}(t) = f_n({}^{n}\mathbf{q}(t), {}^{n}\mathbf{u}(t)), \tag{10b}$$

$$ {}^{1}\mathbf{q}(t), \ldots, {}^{n}\mathbf{q}(t) \in \mathcal{Q}, \, {}^{1}\mathbf{u}(t), \ldots, {}^{n}\mathbf{u}(t) \in \mathcal{U}, \tag{10c}$$

$$\exists k \in [n] \text{ s.t. } {}^{k}\mathbf{b}_{\text{SoC}}(t_f) \in (0, b_f], \tag{10d}$$

$$\forall k \; \mathcal{E}(\boldsymbol{\delta}, {}^{k}\mathbf{q}(t)) \leq \gamma, \tag{10e}$$

$$g_1(\boldsymbol{\delta}, {}^{1}\mathbf{q}(t), {}^{1}\mathbf{u}(t)) \leq 0, \ldots, g_n(\boldsymbol{\delta}, {}^{n}\mathbf{q}(t), {}^{n}\mathbf{u}(t)) \leq 0, \tag{10f}$$

$$ {}^{1}\mathbf{q}(t_0), {}^{1}\mathbf{q}(t_f), \ldots, {}^{n}\mathbf{q}(t_0), {}^{n}\mathbf{q}(t_f), b_f, \gamma \text{ are given}, \tag{10g}$$

where constraints in Eq. (10f) are optional and express additional requirements, e.g., that there is always at least one agent exploring $\mathcal{Q}$, the agents explore the space two-by-two, etc. (see Sec. IV).

Furthermore, the evolutions of the agents' states in time are described by the deterministic nonlinear equation ${}^{k}\dot{\mathbf{q}}(t) = f_k({}^{k}\mathbf{q}(t), {}^{k}\mathbf{u}(t)) \; \forall k \in [n]$ [12].

In Eq. (10), the ergodic metric is integrated into the constraint as proposed in [14].

B. Battery modeling

To derive a battery model for continuous exploration – a model that allows us to predict when an agent is exploring and when it conversely should be recharging the battery – let us consider an equivalent circuit model (ECM). These models are commonly employed in battery metrics estimation for robots and other applications, especially if equipped with rechargeable battery cells [29, 34–38].

The ECM model we employ is a second-order RC model [32], as illustrated in Figure 1 [39].

Formally, it can be formulated as [32]

$$\dot{\mathbf{b}}(t) = \begin{bmatrix} -1/(R_1 C_1) & 0 & 0 \\ 0 & -1/(R_2 C_2) & 0 \\ 0 & 0 & 0 \end{bmatrix} \mathbf{b}(t) - \begin{bmatrix} -1/C_1 \\ -1/C_2 \\ \zeta/Q \end{bmatrix} I(t), \tag{11}$$

where $\zeta \in \mathbb{R}$ is a battery coefficient [29], $R_1, R_2 \in \mathbb{R}$ and $C_1, C_2 \in \mathbb{R}$ are the resistors and capacitors relative to the first and second RC elements in the ECM measured in ohms and farad respectively. $Q \in \mathbb{R}$ is the battery nominal capacity measured in amperes per hour.

$I \in \mathbb{R}$ is then the internal current which is load-dependent, e.g., the current required to run the motors, actuators, etc.

The state $\mathbf{b} := \begin{bmatrix} V_1 & V_2 & \mathbf{b}_{\text{SoC}} \end{bmatrix} \in \mathbb{R}^3$ contains three battery metrics. $V_1, V_2 \in \mathbb{R}$ are the voltages measured in volts across the first and second RC elements, and $\mathbf{b}_{\text{SoC}} \in (0, 1]$ is the normalized battery SoC that evolves from fully charged – or from a given initial value $\mathbf{b}_{\text{SoC}}(t_0)$ – to discharged.

The battery voltage at the extremes of the ECM $V_e \in \mathbb{R}$, measured in volts, can be then formulated as [32]

$$V_e(t) = V_{\text{OC}}(\mathbf{b}_{\text{SoC}}(t)) - V_1(t) - V_2(t) - I(t)R, \tag{12}$$

where $R \in \mathbb{R}$ is the single resistor measured in ohm in Fig. 1, and V_{OC} is the open circuit voltage. It is a nonlinear function of the battery SoC and can be retrieved from the battery data sheet [37].

The values of R_1, C_1, R_2, C_2, R are identified so that the model output and the physical behavior of the agents are matched as closely as possible [32] (see Sec. IV).

The battery model allows us to determine the battery SoC $\mathbf{b}_{\text{SoC}}$ in Eq. (10d), which is in turn utilized to find the control action $\mathbf{u}(t)$ so that there is at least one agent exploring $\mathcal{Q}$ at all times. This means that when the solution of the OCP in Eq. (10) is evaluated, the battery model in Eq. (11) is integrated for the duration of the horizon, whereas the recharging is approximated linear $\mathbf{b}_{\text{SoC}} = \eta \, \mathbf{b}_{\text{SoC}} + \theta$ for a given $\eta, \theta \in \mathbb{R}$.

IV. EXPERIMENTAL RESULTS

In this section, we discuss our experimental setup and results. Our experiments are implemented first in simulation using MATLAB (R), and physical experiments are implemented in Python and conducted using a set of Crazyflie 2.0 micro aerial vehicles (MAVs). Each MAV is equipped with a positioning and wireless charging decks. Precise positioning of MAVs is achieved via two HTC SteamVR Base Station 2.0 units. Each MAV is then equipped with a one-cell 250 mAh 3.7 volts LiPo battery.

In both cases, the source code[1] is released under the popular non-commercial open-source license CC BY NC-SA 4.0. The solution of the OCP in Eq. (10) relies on two external open-source components from the literature: the popular nonlinear programming solver IPOPT [40] and a software framework for nonlinear optimization called CasADi [41].

We evaluate our approach under two different scenarios. In both the scenarios, we use a three-by-three-meter space $\mathcal{Q}$. The spatial distribution ϕ contains four Gaussians in the GMM in Eq. (1), as illustrated in Fig. 2 (the four cyan empty squares).

Intermittent exploration

In the first scenario, one MAV is positioned on top of a wireless charging station at coordinates $(1.5, 1.5)$. The horizon is set to five minutes and is derived empirically along with battery and recharging coefficients. The battery values used in the scenario are those proposed in [32]. The ergodic trajectories at four different horizons t_0, t_4, t_8, and t_{12} are shown in Fig. 3. For horizons following the first, the past ergodic trajectories are illustrated in gray.

Fig. 2: . . . .
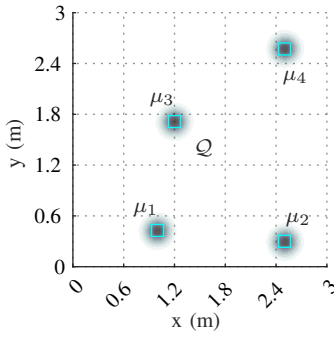
The MAV starts exploring the space (filled blue square in the figure) and derives the ergodic trajectory for the first horizon t_0. At the end of the horizon (filled blue dot), the MAV returns to the charging station. Once the battery is recharged – formally, once the constraint in Eq. (9) is satisfied – the exploration proceeds. The exploration derived in this way is, however, not continuous, as it has periods of "no exploration" in which the agent recharges the battery. We show a continuous exploration achieved by a multi-agent system in the following.

Continuous exploration

In the second extensive scenario, four MAVs α_1, α_2, α_3, and α_4 are placed on top of four wireless charging stations. The optional constraints in Eq. (10f) are built so that each MAV covers two Gaussians at a time that are respectively farthest (μ_3 and μ_2 are the centers of Gaussians covered by the "red" and "dark-green" agents, μ_1 and μ_4 are the centers of the Guassians covered by the "blue" and "magenta" agents), whereas the battery constraint is edited so that there are two MAVs at each time, i.e.,

$$\exists_{=1} k_1, k_2 \in [n] \text{ s.t. } {}^{k_1}\mathbf{b}_{\text{SoC}}, {}^{k_2}\mathbf{b}_{\text{SoC}} \in (0, b_f), \qquad (13)$$

where the notation $\exists_{=1}$ indicates the unique existential quantification.

There is an additional constraint on the final point in Eq (10g), set so that the agent has to be in the proximity of a charging station.

The cost function in Eq. (10a) is further enhanced with the mixing coefficient $\boldsymbol{\delta}$ in Eq. (1), allowing us to find the tradeoffs between the single Gaussians, the different agents, and the battery SoC. Namely, the cost is

$$\min_{\Box, \boldsymbol{\delta}} \frac{1}{n} \sum_{k=1}^{n} \int_{\mathcal{T}_k} {}^{k}\mathbf{u}(\tau)^T R_k {}^{k}\mathbf{u}(\tau) \, d\tau - \frac{1}{n} \sum_{k=1}^{m} \delta_k. \qquad (14)$$

The battery and recharging coefficients are those used in the previous scenario, whereas the horizon is now set to two and a half minutes. The ergodicity metric in Eq. (2) is set to be lower or equal to 0.05 via the constraint in Eq. (10e), in line with similar literature [14].

The results are shown in Fig. 4. The figure is to be read from left to right and from top to bottom, with the horizon being indicated under each subfigure (meaning that t_0 is the first horizon, t_1 is the second horizon, etc.). Initially, two MAVs are selected via the solution to the OCP in Eq. (10), α_1 "blue" and α_2 "red". They are located at coordinates

(0.3,0.9) and (2.7,2.1) respectively, denoted by the blue and red filled squares. The energy-aware ergodic trajectories ${}^{1}\mathbf{q}(t)$ and ${}^{2}\mathbf{q}(t)$ are selected so that the MAVs land at each other's charging stations, i.e., ${}^{1}\mathbf{q}(t_f) = {}^{2}\mathbf{q}(t_0)$ and vice-versa. The mixing coefficients for α_1 are such that $\delta_2 > \delta_3$, meaning that the agent α_1 explores in more detail the area delimited by the Gaussian centered in μ_2. This is indicated by the darker coloring of the different Gaussians, which is proportional to the optimal value of $\boldsymbol{\delta}$.

An analogous situation is to be observed with agent α_2. At the end of the optimization horizon, both agents land in the proximity of each other's charging stations (the red and blue filled dots at the end of the trajectories for respectively α_2 and α_1), meaning that the constraint in Eq. (10g) is evaluated within

$$\| {}^{k_2}\mathbf{q}(t_f) - {}^{k_1}\mathbf{q}(t_0) \| \le \varepsilon, \qquad (15)$$

where $\varepsilon \in \mathbb{R}_{>0}$ and $k_1, k_2 \in [n]$ are given.

Once the two agents α_1 and α_2 land, they start recharging. The formulation of the OCP in Eq. (10) is such that the other two agents α_3 "dark-green" and α_4 "magenta" are selected. They are located at coordinates (0.3,2.1) and (2.7,0.9) respectively. They proceed on the respective energy-aware ergodic trajectories and land at each other's charging stations, with the past trajectory being indicated in the background in gray. The figure shows fourteen horizons. The actual exploration in the scenario, however, is continuous.

V. Conclusion and Future Directions

—

References

[1] H. Choset, "Coverage for robotics–A survey of recent results," *Annals of Mathematics and Artificial Intelligence*, vol. 31, pp. 113–126, 2001. 1

[2] E. Galceran and M. Carreras, "A survey on coverage path planning for robotics," *Robotics and Autonomous Systems*, vol. 61, no. 12, pp. 1258–1276, 2013. 1

[3] T. a. M. Cabreira, L. B. Brisolara, and P. R. Ferreira Jr., "Survey on coverage path planning with unmanned aerial vehicles," *Drones*, vol. 3, no. 1, 2019. 1

[4] I. Abraham, A. Prabhakar, and T. D. Murphey, "An ergodic measure for active learning from equilibrium," *IEEE Transactions on Automation Science and Engineering*, vol. 18, no. 3, pp. 917–931, 2021. 1

[5] L. M. Miller, Y. Silverman, M. A. MacIver, and T. D. Murphey, "Ergodic exploration of distributed information," *IEEE Transactions on Robotics*, vol. 32, no. 1, pp. 36–52, 2016. 1, 2

[6] L. Dressel and M. J. Kochenderfer, "On the optimality of ergodic trajectories for information gathering tasks," in *IEEE American Control Conference*, 2018, pp. 1855–1861. 1

[7] G. De La Torre, K. Flaßkamp, A. Prabhakar, and T. D. Murphey, "Ergodic exploration with stochastic sensor dynamics," in *IEEE American Control Conference*, 2016, pp. 2971–2976. 1

[8] S. Shetty, J. Silvério, and S. Calinon, "Ergodic exploration using tensor train: Applications in insertion tasks," *IEEE Transactions on Robotics*, vol. 38, no. 2, pp. 906–921, 2022. 1

[9] A. Prabhakar, I. Abraham, A. Taylor, M. Schlafly, K. Popovic, G. Diniz, B. Teich, B. Simidchieva, S. Clark, and T. Murphey, "Ergodic specifications for flexible swarm control: From user commands to persistent adaptation," in *Robotics: Science and Systems*, 2020, p. 9. 1

[10] H. Coffin, I. Abraham, G. Sartoretti, T. Dillstrom, and H. Choset, "Multi-agent dynamic ergodic search with low-information sensors," in *IEEE International Conference on Robotics and Automation*, 2022, pp. 11 480–11 486. 1, 2

[1] github.com/adamseew/enerergo

[11] C. Lerch, D. Dong, and I. Abraham, "Safety-critical ergodic exploration in cluttered environments via control barrier functions," in *IEEE International Conference on Robotics and Automation*, 2023, pp. 10 205–10 211. 1

[12] I. Abraham and T. D. Murphey, "Decentralized ergodic control: Distribution-driven sensing and exploration for multiagent systems," *IEEE Robotics and Automation Letters*, vol. 3, no. 4, pp. 2987–2994, 2018. 1, 3

[13] S. Patel, S. Hariharan, P. Dhulipala, M. C. Lin, D. Manocha, H. Xu, and M. Otte, "Multi-agent ergodic coverage in urban environments," in *IEEE International Conference on Robotics and Automation*, 2021, pp. 8764–8771. 1

[14] D. Dong, H. Berger, and I. Abraham, "Time optimal ergodic search," in *Robotics: Science and Systems*, 2023, p. 13. 1, 3, 4

[15] I. Abraham, A. Prabhakar, M. J. Z. Hartmann, and T. D. Murphey, "Ergodic exploration using binary sensing for nonparametric shape estimation," *IEEE Robotics and Automation Letters*, vol. 2, no. 2, pp. 827–834, 2017. 1

[16] A. Rao, A. Breitfeld, A. Candela, B. Jensen, D. Wettergreen, and H. Choset, "Multi-objective ergodic search for dynamic information maps," in *IEEE International Conference on Robotics and Automation*, 2023, pp. 10 197–10 204. 1

[17] E. Ayvali, H. Salman, and H. Choset, "Ergodic coverage in constrained environments using stochastic trajectory optimization," in *IEEE/RSJ International Conference on Intelligent Robots and Systems*, 2017, pp. 5204–5210. 1, 2

[18] G. Mathew and I. Mezić, "Metrics for ergodicity and design of ergodic dynamics for multi-agent systems," *Physica D: Nonlinear Phenomena*, vol. 240, no. 4, pp. 432–442, 2011. 1, 2

[19] L. M. Miller and T. D. Murphey, "Trajectory optimization for continuous ergodic exploration," in *IEEE American Control Conference*, 2013, pp. 4196–4201. 1

[20] C. Di Franco and G. Buttazzo, "Energy-aware coverage path planning of UAVs," in *IEEE International Conference on Autonomous Robot Systems and Competitions*, 2015, pp. 111–117. 1

[21] ——, "Coverage path planning for UAVs photogrammetry with energy and resolution constraints," *Journal of Intelligent & Robotic Systems*, vol. 83, no. 3, pp. 445–462, 2016. 1

[22] I. Shnaps and E. Rimon, "Online coverage of planar environments by a battery powered autonomous mobile robot," *IEEE Transactions on Automation Science and Engineering*, vol. 13, no. 2, pp. 425–436, 2016. 1

[23] T. a. M. Cabreira, C. D. Franco, P. R. Ferreira, and G. C. Buttazzo, "Energy-aware spiral coverage path planning for UAV photogrammetric applications," *IEEE Robotics and Automation Letters*, vol. 3, no. 4, pp. 3662–3668, 2018. 1

[24] M. Wei and V. Isler, "Coverage path planning under the energy constraint," in *IEEE International Conference on Robotics and Automation*, 2018, pp. 368–373. 1

[25] K. R. Jensen-Nau, T. Hermans, and K. K. Leang, "Near-optimal area-coverage path planning of energy-constrained aerial robots with application in autonomous environmental monitoring," *IEEE Transactions on Automation Science and Engineering*, vol. 18, no. 3, pp. 1453–1468, 2021. 1

[26] Y. Mei, Y.-H. Lu, Y. C. Hu, and C. G. Lee, "Energy-efficient motion planning for mobile robots," in *IEEE International Conference on Robotics and Automation*, vol. 5, 2004, pp. 4344–4349. 1

[27] ——, "A case study of mobile robot's energy consumption and conservation techniques," in *IEEE International Conference on Advanced Robotics*, 2005, pp. 492–497. 1

[28] C. H. Kim and B. K. Kim, "Energy-saving 3-step velocity control algorithm for battery-powered wheeled mobile robots," in *IEEE International Conference on Robotics and Automation*, 2005, pp. 2375–2380. 1

[29] A. Seewald, H. García de Marina, H. S. Midtiby, and U. P. Schultz, "Energy-aware planning-scheduling for autonomous aerial robots," in *IEEE/RSJ International Conference on Intelligent Robots and Systems*, 2022, pp. 2946–2953. 1, 3

[30] P. Ondrúška, C. Gurău, L. Marchegiani, C. H. Tong, and I. Posner, "Scheduled perception for energy-efficient path following," in *IEEE International Conference on Robotics and Automation*, 2015, pp. 4799–4806. 1

[31] S. Sudhakar, S. Karaman, and V. Sze, "Balancing actuation and computing energy in motion planning," in *IEEE International Conference on Robotics and Automation*, 2020, pp. 4259–4265. 1

[32] S. Zhao, S. R. Duncan, and D. A. Howey, "Observability analysis and state estimation of lithium-ion batteries in the presence of sensor biases," *IEEE Transactions on Control Systems Technology*, vol. 25, no. 1, pp. 326–333, 2017. 1, 3

[33] S. Calinon, *Mixture models for the analysis, edition, and synthesis of continuous time series.* Springer, 2020, pp. 39–57. 1, 2

[34] C. Zhang, W. Allafi, Q. Dinh, P. Ascencio, and J. Marco, "Online estimation of battery equivalent circuit model parameters and state of charge using decoupled least squares technique," *Energy*, vol. 142, pp. 678–688, 2018. 3

[35] X. Hu, S. Li, and H. Peng, "A comparative study of equivalent circuit models for li-ion batteries," *Journal of Power Sources*, vol. 198, pp. 359–367, 2012. 3

[36] A. Hasan, M. Skriver, and T. A. Johansen, "eXogenous Kalman filter for state-of-charge estimation in lithium-ion batteries," in *IEEE Conference on Control Technology and Applications*, 2018, pp. 1403–1408. 3

[37] H. Hinz, "Comparison of lithium-ion battery models for simulating storage systems in distributed power generation," *Inventions*, vol. 4, 2019. 3

[38] S. Mousavi G. and M. Nikdel, "Various battery models for various simulation studies and applications," *Renewable and Sustainable Energy Reviews*, vol. 32, pp. 477–485, 2014. 3

[39] A. Seewald, "Energy-aware coverage planning and scheduling for autonomous aerial robots," Ph.D. dissertation, Syddansk Universitet. Det Tekniske Fakultet, 2021, doi.org/10.21996/7ka6-r457. 3

[40] A. Wächter and L. T. Biegler, "On the implementation of an interior-point filter line-search algorithm for large-scale nonlinear programming," *Mathematical Programming*, vol. 106, no. 1, pp. 25–57, 2006. 3

[41] J. Andersson, J. Åkesson, and M. Diehl, "CasADi: A symbolic package for automatic differentiation and optimal control," in *Recent Advances in Algorithmic Differentiation.* Springer, 2012, pp. 297–307. 3

Fig. 3: . . . .

Fig. 4: ....
....
....
....
....
....
....
....
....
....
....
....
....
....